ACS Partner Journal

CHEMICAL & BIOMEDICAL IMAGING

pubs.acs.org/ChemBioImaging

Article

Fluorogenic Linkage Integration for Nonfluorescent Transformations (FLINT)

Published as part of Chemical & Biomedical Imaging special issue "Imaging in Energy Science".

Bishal Pokhrel,[‡] Fatiha Farhana,[‡] Li Zuo,[‡] Rebecca L. Stratton, Pravin Pokhrel, Mohammad Akter Hossain, Jiahao Ji, Hanbin Mao, and Hao Shen*

Cite This: *Chem. Biomed. Imaging* 2025, 3, 253−259

Read Online

ACCESS | Metrics & More | Article Recommendations | Supporting Information

ABSTRACT: Since its creation, single-molecule optical imaging has revolutionized the study of catalytic processes, yet its application largely relies on probing fluorogenic reactions. To overcome this limitation, we propose the Fluorogenic Linkage Integration for Nonfluorescent Transformation (FLINT) approach, an imaging method to resolve nonfluorogenic reactions at the single-molecule level. Using glucose oxidation as a model reaction, we coupled this nonfluorogenic reaction with a fluorogenic Amplex Red (AR) → resorufin (RF) transformation to create a cascading reaction. This integration allowed us to monitor single-turnover events and extract key kinetic parameters for glucose oxidation despite their being invisible under the optical microscope. Our ensemble measurements combining cyclic voltammetry and fluorescence spectroscopy confirmed the cascade reaction mechanism and revealed first-order kinetics for both elementary reaction steps. At the single-molecule level, turnover time analysis provided detailed information on the reaction kinetics, distinguishing the relatively fast glucose oxidation from slower AR oxidation. We further confirmed the validity of the FLINT approach by comparing the catalytic performances of 5 nm gold nanoparticles (AuNPs) against that of 18 × 52 nm gold nanorods (AuNRs) and AuNP@DNA coronazymes. Furthermore, FLINT was used to evaluate the chiral selectivity of D- and L-glucose on coronazymes, suggesting the potential application of FLINT in enantioselective reactions. The FLINT approach is a significant advancement in single-molecule imaging as it enables the study of nonfluorogenic reactions with high spatiotemporal resolution.

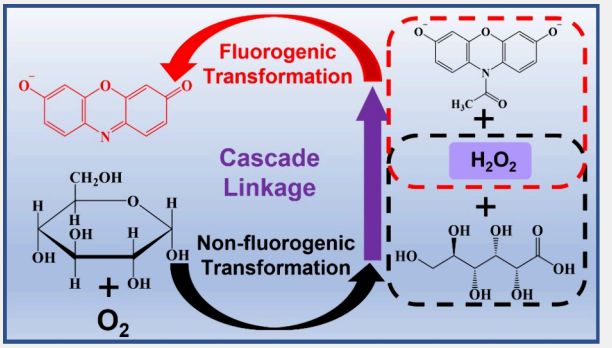

KEYWORDS: *Single-Molecule, Fluorogenic Linkage, Nonfluorogenic Reactions, Glucose Oxidation, Reaction Kinetics*

1. INTRODUCTION

Single-molecule optical imaging has gained significant attention since its invention, mainly due to its ability to perform noninvasive and nondestructive observations in real-time.[1−3] Unlike conventional characterization methods, which often rely on ensemble measurements, the single-molecule approach examines individual target species one at a time. This unique capability enables the identification of critical kinetic steps and the elucidation of subpopulations that are otherwise obscured by ensemble averaging. The development and subsequent advancements in super-resolution imaging techniques have further revolutionized this field by surpassing the diffraction limit of conventional optical systems.[4−6] These developments have elevated the spatial resolution of single-molecule imaging to the subdiffraction level, allowing researchers to visualize molecular interactions and dynamics with unprecedented clarity.

Due to its exceptional spatiotemporal resolution, the single-molecule optical imaging techniques have rapidly become a cornerstone in biochemical research, offering insights into fundamental biological processes at the molecular scale.[7,8] Beyond biochemistry, its applications extend to various fields, including enzymology,[9] heterogeneous catalysis,[10] polymer science,[11] and materials chemistry.[6] By enabling precise and detailed analysis across these fields, single-molecule imaging continues to play a transformative role in advancing scientific understanding and innovation.

Detecting optical signals from a single molecule is inherently challenging due to the extremely low signal strengths.[12,13] As a result, most single-molecule-based optical techniques rely on the detection of relatively strong fluorescence signals.[14−17]

Received: December 30, 2024
Revised: February 20, 2025
Accepted: February 21, 2025
Published: March 3, 2025

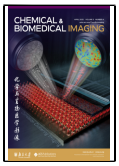

This necessitates fluorescent labeling of the specimen to facilitate imaging or the use of fluorogenic probes when studying chemical transformations. Fluorescence-based methods are favored for their high sensitivity and ability to achieve superior spatiotemporal resolution. In addition to fluorescence detection, other single-molecule techniques have been developed that exploit signals such as absorption spectroscopy,[18,19] Raman scattering,[20,21] force response,[22,23] or electrochemical signals.[24−26] These approaches offer complementary insights and can be equally powerful and informative in specific contexts. However, due to their inherently weaker responses compared to fluorescence emission, these alternative methods often face limitations in achieving the same level of spatial and temporal resolution.

Most chemical and biological processes do not inherently involve fluorescent functionalities, posing a significant challenge to extending established single-molecule methods to study such systems. To address the reliance on fluorescent labels, several label-free single-molecule detection techniques have been developed over the past two decades. These methods utilize phenomena such as resonance shifts upon molecular binding,[27] plasmonic resonances,[28,29] competitive binding,[30] and light-molecule interactions.[31] While these label-free approaches have shown great promise, achieving comparable spatiotemporal resolution to fluorescence-based techniques remains a key challenge. The ability to perform high-resolution detection for nonfluorescent processes is still highly desired to date.

In this work, we introduce the Fluorogenic Linkage Integration for Nonfluorescent Transformation (FLINT) approach as a novel method to detect nonfluorogenic chemical reactions at the single-molecule level. To demonstrate the efficacy of FLINT, we employed glucose conversion - a reaction commonly catalyzed by glucose oxidase[32,33] - as a model system. By coupling the nonfluorogenic glucose oxidation reaction with a fluorogenic probe through a cascading reaction mechanism, we enabled the optical imaging of reaction kinetics at the single catalyst, single turnover level. The cascading reaction was rigorously evaluated at both the ensemble and single-molecule levels to confirm the successful integration of the two reaction processes. Importantly, our results demonstrate that the nonfluorogenic glucose oxidation can be fully resolved at the single-catalyst level through turnover time analysis. To further validate the utility of the FLINT approach, we investigated and compared the catalytic performances of three distinct types of nanocatalysts in glucose oxidation, providing key insights into their efficiency and behavior. Furthermore, FLINT is not confined to glucose oxidation; any nonfluorogenic reaction that can be linked with a fluorogenic reaction is amenable to FLINT. Examples include ROS formation (e.g., alcohol oxidation,[34,35] alkaline phosphatase conversion,[36] and chemical ligation reactions.[37]

2. EXPERIMENTAL SECTION

2.1. Materials

Citrate-capped gold nanoparticles (AuNPs) (5 nm) were acquired from Nanocomposix, San Diego, CA. Citrate-capped gold nanorods (AuNRs, 18 × 52 nm) were purchased from Nanopartz, Loveland, CO. All oligonucleotides were obtained from Integrated DNA Technologies (IDT, Coralville, IA) and purified using denaturing polyacrylamide gels, followed by ethanol precipitation. All enzymes were purchased from New England Biolabs (NEB Inc., Ipswich, MA). Hydrogen peroxide solution (30%) was purchased from Spectrum Chemical Corp. Amplex Red (AR) powder was purchased from Invitrogen. D-Glucose (anhydrous, 99%) was purchased from Thermo Fisher Scientific and L-glucose (purity >98%) was purchased from Tokyo Chemical Industry Co. Ltd. Sodium hydrogen phosphate and sodium dihydrogen phosphate were purchased from Sigma-Aldrich. Unless otherwise stated, all chemicals were used as received.

2.2. Ensemble Electrochemistry Measurement

An electrochemical cell was constructed by connecting three electrodes to a CHI1200E potentiostat (CH Instruments). Five nm AuNPs were dropcasted to a glassy carbon electron to form the working electrode, while a platinum wire served as the counter electrode and Ag/AgCl electrode served as the reference electrode. The electrochemical cell was filled with 50 mM phosphate buffer at pH 7.4. For the calibration of hydrogen peroxide (H_2O_2), 1.0−5.5 mM H_2O_2 solution was prepared. Cyclic voltammetry (CV) measurements were performed by sweeping the potential between 0.0 and 1.2 V, and the resulting current was recorded. A calibration curve for H_2O_2 concentration was generated based on the measured voltammograms.

2.3. Ensemble Catalytic Measurement

The oxidation of glucose by molecular oxygen and catalyst generates H_2O_2, which could readily react with AR to form the highly fluorescent resorufin (RF). To carry out this cascade reaction, a pH 7.4, 50 mM phosphate buffer was presaturated with O_2. Twenty mM glucose, 10 μM μM AR and 5 nm AuNPs were added to the buffer to form a reaction mixture. The fluorescence signal escalated as the reaction proceeded. An Agilent Cary60 fluorometer was used to record the fluorescent emission of the reaction product.

2.4. Synthesis of DNA@AuNP Coronazyme

The preparation of DNA@AuNP has been detailed in our previous studies.[38,39] Briefly, a poly(A) sequence has been integrated into a DNA hairpin for the 5 nm AuNP binding. The poly(A)-DNA replaces the citrate ligand on AuNP through a freeze−thaw procedure: the poly(A)-DNA was mixed with citrate-capped AuNP colloidal solution in a 1:10 molar ratio. This mixture was kept at −80 °C for ∼15 min and then quickly thawed at room temperature to redistribute the particles. The poly(A)-DNA replaced the citrate and stabilized the AuNPs from aggregation.

2.5. Single-Molecule Measurement

For single-molecule catalytic measurements, nanocatalysts were immobilized on a coverslip and assembled into a custom microfluidic chamber with continuous tubing for reaction mixture supply. The reaction mixture, containing 0−30 mM glucose and 50−2000 nM AR, was prepared in 50 mM phosphate buffer at pH ∼7.4. To ensure oxygen saturation, the reaction reservoir was continuously purged with O_2 before injection into the chamber.

Excitation was achieved using a 532 nm continuous-wave laser (DragonLaser) with ∼8 mW power. An oil-immersion 100× N.A. 1.49 objective (UAPON 100xOTIRF, Olympus) was used to construct an objective-type total internal reflection fluorescence (TIRF) setup. The emitted signals were filtered with a bandpass filter (Chroma ET575/50 m) and a long-pass filter (Chroma ET542lp), then captured using an sCMOS camera (Photometrics Prime 95B) at a frame rate of 20−50 fps through Olympus CellSens Dimension software.

2.6. Single-Molecule Image Analysis

Image analysis was performed with ThunderSTORM,[40] an ImageJ plugin, and further processed with a custom-written MATLAB program to localize individual fluorescent product molecules.

3. RESULTS AND DISCUSSION

Glucose, in the presence of oxygen (O_2) and a glucose oxidase-mimicking catalyst, undergoes oxidation to produce gluconic acid, with H_2O_2 as a byproduct (Figure 1A). The stoichiometric ratio between glucose and H_2O_2 is 1:1. When multifunctional nanocatalysts, such as gold nanoparticles

https://doi.org/10.1021/cbmi.4c00114
Chem. Biomed. Imaging 2025, 3, 253−259

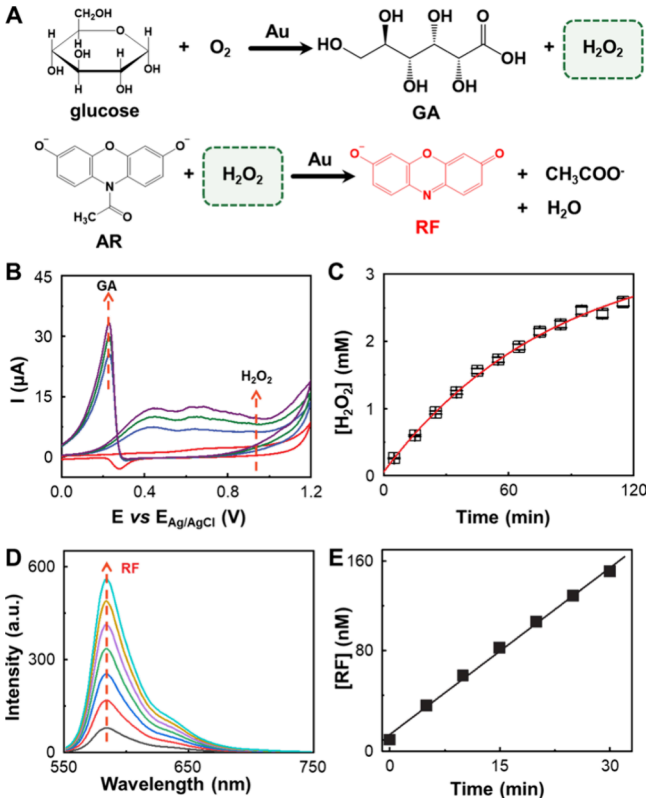

Figure 1. Cascade reaction design to probe glucose oxidation at the ensemble level. (A) Schematic representation of the cascade reaction where glucose oxidation produces H_2O_2, which subsequently facilitates the oxidation of AR to generate the fluorescent product RF. (B) Cyclic voltammograms of the reaction mixture containing 20 mM glucose in oxygen-saturated phosphate buffer. As the reaction proceeds, the redox peaks corresponding to glucose oxidation (~0.23 V, red arrow) and H_2O_2 oxidation (~0.95 V, red arrow) increase in intensity. (C) Time-dependent H_2O_2 concentration changes during glucose oxidation. The H_2O_2 concentration was determined from the cyclic voltammetry current response by referencing the H_2O_2 working curve. The red line represents a fit to a first-order kinetic model. (D) Fluorescence spectra of the reaction mixture (20 mM glucose and 10 μM AR in oxygen-saturated phosphate buffer) as the cascade reaction progresses. The red arrow highlights the peak emission of RF (~580 nm). (E) Time-dependent RF concentration changes during the cascade reaction. The black line represents a linear fit to the data, indicating the progression of the AR → RF transformation.

(AuNPs), is introduced, the reaction does not terminate at the formation of H_2O_2. Instead, the AuNPs can further catalyze the decomposition of H_2O_2 into radical species.[41,42] This catalytic feature enables the integration of glucose oxidation with the oxidation of the radical probe, Amplex Red (AR), to produce the highly fluorescent product resorufin (RF). It is noteworthy that in the absence of glucose and the subsequent transformation, oxygen alone cannot oxidize AR in the presence of AuNPs. Therefore, the cascade reaction is essential for the generation of RF.

To investigate the reaction kinetics of the cascade process, we employed cyclic voltammetry (CV) and fluorescence spectroscopy to monitor the formation of H_2O_2 and RF, respectively. Both glucose and H_2O_2 are electrochemically active, allowing for the quantification of their formation during the catalytic transformation.[43,44] For H_2O_2 calibration, an AuNP working electrode was prepared by depositing AuNPs onto a glassy carbon electrode. Pure H_2O_2 solutions at various concentrations were analyzed via cyclic voltammetry, utilizing a platinum counter electrode and an Ag/AgCl reference electrode. The cyclic voltammograms revealed a distinct oxidation peak for H_2O_2 at approximately 0.95 V.[45] The current response exhibited a linear dependence on H_2O_2 concentration, enabling the establishment of a standard working curve for subsequent quantitative analysis (Supporting Information Figure S1).

To probe glucose oxidation, we assembled an electrochemical cell containing glucose in O_2-saturated phosphate buffer. In the absence of externally added H_2O_2, the characteristic H_2O_2 oxidation peak at ~0.95 V was observed, indicating the in situ formation of H_2O_2 as a product of glucose oxidation. Additionally, another oxidation peak appeared at ~0.23 V, which was attributed to gluconic acid formation (Figure 1B).[44] By referencing the H_2O_2 calibration curve, we quantitatively monitored the progress of glucose oxidation. The results showed that the H_2O_2 concentration increased over time, eventually reaching a plateau after approximately 2 h (Figure 1C). The time-dependent concentration profile revealed that glucose oxidation followed first-order reaction kinetics, with a rate constant of 4.0×10^{-4} s^{-1}. This reaction kinetics is further confirmed by the gluconic acid formation at ~0.23 V (Supporting Information Figure S2).

Once glucose oxidation was integrated with the AR → RF transformation, the progress of the cascade reaction was monitored through the increase in fluorescence intensity of the reaction mixture, as RF exhibits strong emission peaking at ~580 nm (Figure 1D).[46,47] The fluorescence intensity increased linearly over time, consistent with the progression of the cascade reaction. Previous studies have shown that the AR → RF transformation follows first-order kinetics.[42,47] In our measurements, the RF formation displayed a linear dependence on reaction time, suggesting a relatively slow reaction rate (Figure 1E). The rate constant for the cascade reaction was determined to be 4.2×10^{-6} s^{-1}, which was significantly lower than that of glucose oxidation alone. This difference highlights that AR oxidation is the rate-limiting step in the cascade reaction.

Since both glucose oxidation and AR oxidation are pseudo-first-order reactions, the overall cascade reaction also exhibits apparent first-order kinetics, dominated by the slower AR oxidation step. The measured kinetics (Figure 1E) primarily reflect the AR oxidation process, providing valuable insight into rate-limiting behavior within the integrated cascade reaction.

To perform the cascade reaction at the single-molecule level, AuNPs were immobilized onto a microscope coverslip, which was then incorporated into a microfluidic device (Figure 2A). In the absence of either glucose or AR in the reaction mixture, no fluorescence signals were observed, as the fluorescence linkage between glucose oxidation and AR oxidation was not established. However, when both glucose and AR were present in an oxygen-saturated buffer solution, repetitive fluorescence spots appeared within the field of view, corresponding to the formation of RF through the cascade reaction. Notably, these fluorescence images are compatible with super-resolution imaging algorithms. For larger nanocatalysts, FLINT can therefore map the distribution of reactive sites at approximately 20 nm spatial resolution.[48,49] By analyzing the waiting time between consecutive RF formation events at the same catalyst, the microscopic turnover time (τ) for a single catalyst was determined (Figure 2B). The statistical distribution of τ

https://doi.org/10.1021/cbmi.4c00114
Chem. Biomed. Imaging 2025, 3, 253−259

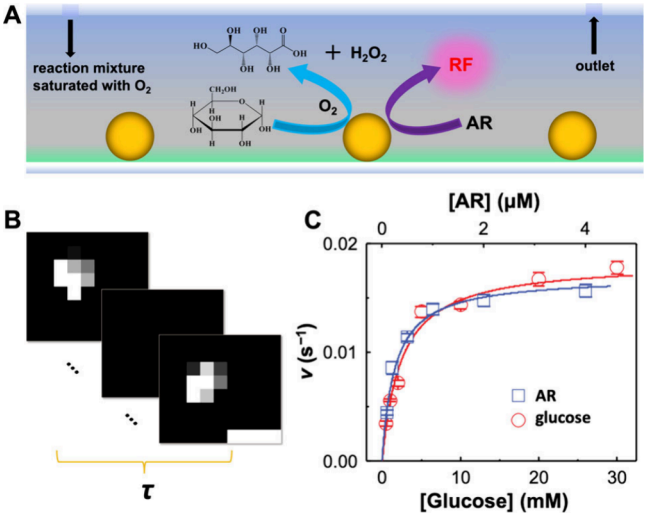

Figure 2. (A) Schematic of the single-molecule design of FLINT imaging for glucose oxidation. (B) Schematic of extracting the τ from a single AuNP catalyst. Each frame is a fluorescence image at the location of a AuNP catalyzing the cascade reaction. Scale bar is 500 nm. (C) The reaction rate dependence on glucose and AR concentrations, respectively. Solid lines are global fits using the Langmuir–Hinshelwood model.

values provided insight into the catalytic behavior of the individual catalyst.[5,10]

To further investigate the kinetics of the cascade reaction, we conducted substrate concentration titration experiments for both glucose and AR. It was found that the reactivity of AuNPs were highly heterogeneous, evidenced by the broad turnover rate distributions for individual catalysts (Supporting Information Figure S3). During each titration, the concentration of the other substrate was maintained at a high level to ensure it was not the limiting reagent. The results showed that the reaction rate increased with increasing substrate concentration for both glucose and AR, consistent with the characteristics of Langmuir–Hinshelwood kinetics (Figure 2C).[50,51] The presence of saturation regions in both titration curves indicated that glucose and AR adsorb onto distinct surface sites of the AuNP catalyst. If competitive adsorption had occurred, a decrease in the turnover rate would have been observed at high substrate concentrations.[52]

Using the Langmuir–Hinshelwood model, we derived a kinetic equation to describe the cascade reaction (Supporting Information Section 4):

$$\langle\tau\rangle^{-1} = k_{\text{eff}}\frac{K_{\text{G}}K_{\text{AR}}[\text{glucose}][\text{AR}]}{(1 + K_{\text{G}}[\text{glucose}])(1 + K_{\text{AR}}[\text{AR}])} \quad (1)$$

In this equation, $\langle\rangle$ denotes averaging, k_{eff} is the effective rate constant for the cascade reaction for a single reactive site, K_{G} and K_{AR} are the adsorption/desorption equilibrium constants for glucose and AR, respectively; [glucose] and [AR] are the glucose and AR concentrations in the solution. Using eq 1 to globally fit the titration data in Figure 2C, we found $k_{\text{eff}} = 0.021 \pm 0.001\ \text{s}^{-1}$ particle^{-1}, $K_{\text{G}} = 0.38 \pm 0.04\ \text{mM}^{-1}$, and $K_{\text{AR}} = 4.39 \pm 0.38\ \mu\text{M}^{-1}$. These values were in excellent agreement with the kinetics observed independently using electrochemistry and fluorescence spectroscopy at the ensemble level. This further confirmed that the overall kinetics of the cascade reaction are dominated by the relatively slower AR oxidation step.

The single-molecule cascade reaction enables detailed kinetic analyses for individual catalysts. For a 5 nm AuNP catalyzing a first-order fluorogenic reaction such as AR → RF, the distribution of turnover times follows a single exponential decay.[25,51] The decay constant directly provides the rate constant for this catalyst (Figure 3A and B). However, if the

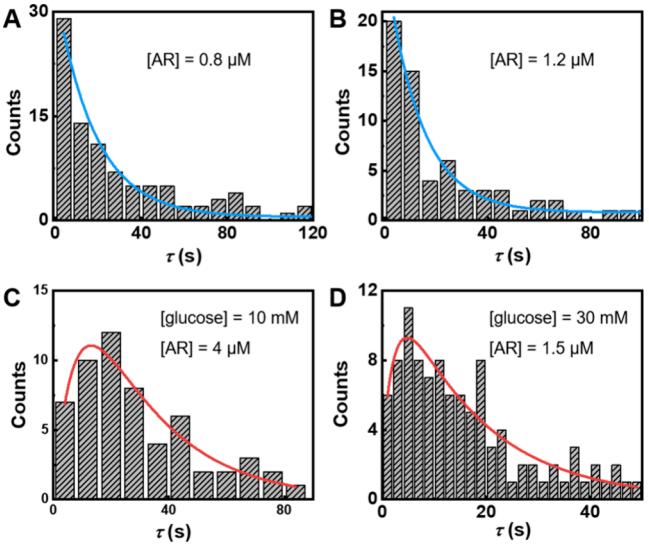

Figure 3. Distributions of turnover time τ for 5 nm AuNPs. (A, B) AR reacts with 60 mM H_2O_2 in pH 7.4 phosphate buffer. The reaction follows first-order kinetics. Blue curves are single-exponential decay functions with decay constants 0.055 and 0.074 s^{-1}, respectively. (C, D). Cascade glucose oxidation at different substrate concentrations. Red curves are fits using biexponential functions. $k_1 = 0.177\ \text{s}^{-1}$, $k_2 = 0.053\ \text{s}^{-1}$ (C). $k_1 = 0.424\ \text{s}^{-1}$, $k_2 = 0.062\ \text{s}^{-1}$ (D).

fluorogenic conversion involves two rate-limiting steps—such as the formation of an intermediate species followed by its consumption to produce the final product—the τ distribution exhibits biexponential behavior (Figure 3C and D).[42,51] This phenomenon has been previously reported in both single-molecule enzymatic and nanoparticle catalysis, even when the intermediate species are nonfluorescent.[42,53] The key criterion for observing biexponential behavior is the detector's ability to capture both rate-limiting steps with sufficient temporal resolution.

In our cascade reaction, H_2O_2 serves as the intermediate species, resulting in a biexponential turnover time distribution. By fitting the distribution with the equation $f(\tau) = A(e^{-k_1\tau} - e^{-k_2\tau})$, we extracted two apparent rate constants, k_1 and k_2, corresponding to the two elementary steps in the reaction. It was observed that the value of k_1 is about 1 order of magnitude higher than k_2. This observation aligns with ensemble measurements, where glucose oxidation was significantly faster than AR oxidation. Accordingly, k_1, which corresponds to the rapid rising phase in the histogram, is attributed to glucose oxidation. Conversely, k_2, corresponding to the slower decay phase, is attributed to the subsequent AR oxidation (Figure 3C and D).

A key advantage of single-molecule turnover time analysis is its ability to provide kinetic information about nonfluorescent reactions, such as glucose oxidation, even when no direct fluorescent product is involved. This level of detail cannot be achieved through ensemble measurements, as demonstrated in Figure 1. It is important to note that as apparent rate constants,

https://doi.org/10.1021/cbmi.4c00114
Chem. Biomed. Imaging 2025, 3, 253–259

k_1 and k_2 may vary depending on the concentrations of glucose and AR until saturation is reached (Figure 4). This is because

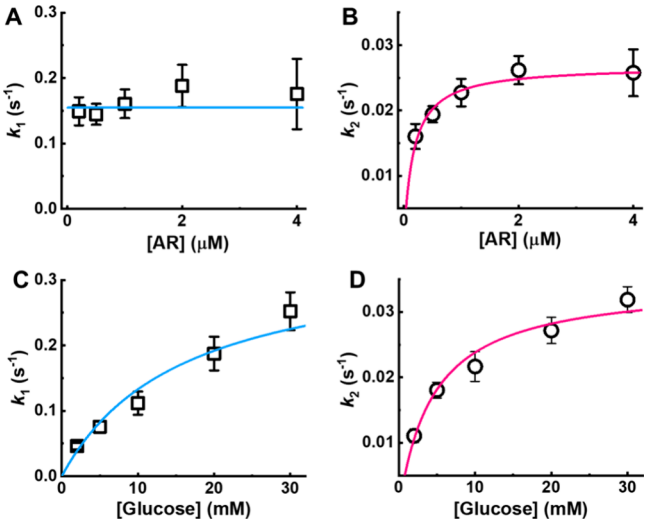

Figure 4. Extracted kinetic parameters from the single AuNP-catalyzed cascade reaction. (A, B) The extracted k_1 (A) and k_2 (B) from AR concentration titration. (C, D) The extracted k_1 (C) and k_2 (D) from AR concentration titration. The gradual increase in B, C, and D represent the gradual occupation of surface sites. The solid fits in them are fits using derived Langmuir−Hinshelwood equations (Supporting Information Section 4). Error bars are s.e.m.

each nanocatalyst contains multiple reactive sites on its surface, and the apparent k_1 and k_2 are products of the per-site reactivity and the number of occupied sites (Supporting Information Section 5). According to the Langmuir−Hinshelwood model, the number of occupied sites is dependent on substrate concentration.[50,51] Consequently, k_1 and k_2 are concentration-dependent until a threshold concentration is achieved, where all surface sites are occupied (Figure 4). For our cascade reaction, the threshold concentrations were determined to be greater than 30 mM for glucose and greater than 2 μM for AR. Beyond these concentrations, the k_1 and k_2 values represent the maximum reactivity (k_{eff}, Supporting Information Section 5) for glucose and AR oxidation, respectively. Under these saturated conditions, k_1 and k_2 provide a reliable measure of the catalytic reactivity of the nanocatalysts.

The integration of the cascade reaction design and single-molecule analysis formulates the FLINT approach, enabling the evaluation of nanocatalyst reactivity. Using the FLINT approach, we compared the reactivity of 5 nm AuNPs and 18 × 52 nm AuNRs. It was observed that AuNRs exhibited slightly higher reactivity than AuNPs, as evidenced by larger k_1 and k_2 values (Figure 5). This enhancement is likely attributable to the larger surface area of AuNRs, which provides more surface sites for substrate interactions.

Interestingly, a significant increase in reactivity was observed when DNA hairpins were attached to the 5 nm AuNPs, generating coronazymes (Figure 5). Our previous studies have suggested that the DNA corona surrounding the AuNP core facilitates long-range catalysis directly on the DNA strands.[39] Such long-range catalysis stems from strong DNA corona-substrate interaction, forcing the catalytic conversion to occur exclusively at DNA binding sites. This long-range catalysis appeared to contribute to glucose oxidation, as the k_1 value for

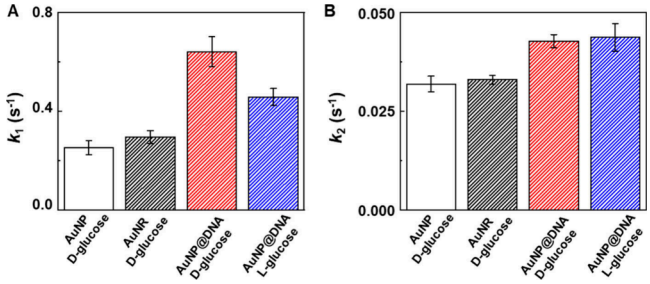

Figure 5. Reactivity comparison for different nanocatalysts in catalyzing the cascade glucose oxidation. (A) k_1 and (B) k_2 values were extracted from the waiting time distribution from individual catalysts. Each bar is an average of more than 50 catalysts. Error bars are s.e.m. [glucose] = 30 mM, [AR] = 2 μM.

the AuNP@DNA coronazyme was ∼2.54 times greater than that of the bare 5 nm AuNP. The subsequent AR oxidation step also showed improvement, but the enhancement was less pronounced compared to glucose oxidation. This is likely because, although the DNA corona enhances AR binding, the radical generation following H_2O_2 formation is still catalyzed by the AuNP core. As a result, the increment in k_2 was relatively small.

It is worth noting that glucose is a chiral substrate with two enantiomers, D-glucose and L-glucose. For AuNPs and AuNRs, only D-glucose was tested, as these nanocatalysts are achiral. However, the coronazyme, which contains a chiral DNA ligand, has the potential to selectively interact with the two enantiomers. To investigate this, we employed the FLINT method to evaluate the conversion of L-glucose on coronazyme (Figure 5). The results showed that k_1 was lower for L-glucose compared to D-glucose, likely due to the mismatch between the left-handed L-glucose and the right-handed DNA strands in the corona. In contrast, the k_2 values for D- and L-glucose were statistically indistinguishable. This is expected because second-stage AR oxidation is achiral, and thus the apparent rate constants remain unaffected by the chirality of glucose. The comparison of different nanocatalysts and glucose enantiomers demonstrates the effectiveness of the FLINT approach in evaluating the catalytic capabilities of nanocatalysts in nonfluorogenic reactions.

4. CONCLUSION

In this work, we developed the FLINT approach, an imaging method that extends the capacity of single-molecule optical imaging into nonfluorogenic reactions. By combining non-fluorogenic glucose oxidation with a fluorogenic AR → RF transformation, we created a cascade reaction capable of resolving single reaction turnovers for individual nanocatalysts. By performing comprehensive analyses at both ensemble and single-molecule levels, we validated the kinetics of the cascade reaction. H_2O_2, as the byproduct of glucose, served as an intermediate species, bridging up the two elementary steps in this cascade reaction. The FLINT approach reached its full potential at the single-molecule level, because even in the absence of a direct fluorescent product, the analyses of turnover time revealed the kinetics of nonfluorogenic glucose oxidation. This highlights the unique power of the FLINT approach to resolve and quantify nonfluorogenic reactions that are otherwise inaccessible through conventional techniques.

With the development of FLINT approach, we systematically compared the catalytic reactivity of 5 nm AuNPs, 18 × 52

https://doi.org/10.1021/cbmi.4c00114
Chem. Biomed. Imaging 2025, 3, 253−259

nm AuNRs, and AuNP@DNA coronazymes in catalyzing glucose oxidation. It was found that AuNRs exhibited slightly higher reactivity than 5 nm AuNPs because of their larger surface area and more reactive sites. However, the integration of DNA hairpins into the coronazyme significantly enhanced the catalyst's reactivity in glucose oxidation. This enhancement is attributed to DNA corona's ability to bind more reaction substrates and enable long-range catalysis directly within the corona phase. Moreover, FLINT revealed that D/L-glucose enantiomers displayed different reactivity on coronazymes, suggesting potential applications of the FLINT approach in probing chiral selective reactions at the molecular level.

The development of the FLINT approach is a significant advancement in single-molecule optical imaging, since it overcomes the limitations associated with nonfluorescent chemical reactions. More importantly, single-molecule turnover analysis fully harnessed FLINT's capabilities, offering complete reaction kinetics for individual nanocatalysts. We anticipate that this method will broaden the scope of single-molecule studies, enabling detailed investigation of various chemical transformations previously inaccessible with conventional fluorescence-based techniques.

■ ASSOCIATED CONTENT

Supporting Information

The Supporting Information is available free of charge at https://pubs.acs.org/doi/10.1021/cbmi.4c00114.

Calibration of H_2O_2 concentration, electrochemical conversion of GA, reactivity heterogeneity among 5 nm AuNPs, derivation of the Langmuir−Hinshelwood equation for the cascade reaction, kinetic equation under limiting conditions, turnover time distribution, and probability density function (PDF)

■ AUTHOR INFORMATION

Corresponding Author

Hao Shen − *Department of Chemistry and Biochemistry and Advanced Materials and Liquid Crystals Institute, Kent State University, Kent, Ohio 44242, United States;* orcid.org/0000-0002-2798-5861; Email: hshen7@kent.edu

Authors

Bishal Pokhrel − *Department of Chemistry and Biochemistry, Kent State University, Kent, Ohio 44242, United States*

Fatiha Farhana − *Department of Chemistry and Biochemistry, Kent State University, Kent, Ohio 44242, United States*

Li Zuo − *Department of Chemistry and Biochemistry, Kent State University, Kent, Ohio 44242, United States*

Rebecca L. Stratton − *Department of Chemistry and Biochemistry, Kent State University, Kent, Ohio 44242, United States;* orcid.org/0009-0001-8005-7327

Pravin Pokhrel − *Department of Chemistry and Biochemistry, Kent State University, Kent, Ohio 44242, United States;* orcid.org/0000-0003-4259-6087

Mohammad Akter Hossain − *Department of Chemistry and Biochemistry, Kent State University, Kent, Ohio 44242, United States*

Jiahao Ji − *Department of Chemistry and Biochemistry, Kent State University, Kent, Ohio 44242, United States;* orcid.org/0000-0002-6189-7750

Hanbin Mao − *Department of Chemistry and Biochemistry and Advanced Materials and Liquid Crystals Institute, Kent State University, Kent, Ohio 44242, United States;* orcid.org/0000-0002-6720-9429

Complete contact information is available at: https://pubs.acs.org/10.1021/cbmi.4c00114

Author Contributions

‡B.P., F.F., and L.Z. contributed equally.

Notes

The authors declare no competing financial interest.

■ ACKNOWLEDGMENTS

The authors acknowledge the National Science Foundation (NSF) (No. CHE2247709) for grant support. H.M. acknowledges the National Institute of Health (NIH) (No. R01 CA252827). H.S. acknowledges Kent State University's Farris Family Foundation for grant support.

■ REFERENCES

(1) Lelek, M.; Gyparaki, M. T.; Beliu, G.; Schueder, F.; Griffié, J.; Manley, S.; Jungmann, R.; Sauer, M.; Lakadamyali, M.; Zimmer, C. Single-molecule localization microscopy. *Nature Reviews Methods Primers* **2021**, *1* (1), 39.

(2) Shashkova, S.; Leake, M. C. Single-molecule fluorescence microscopy review: shedding new light on old problems. *Biosci. Rep.* **2017**, *37* (4), BSR20170031.

(3) Moerner, W. E.; Fromm, D. P. Methods of single-molecule fluorescence spectroscopy and microscopy. *Rev. Sci. Instrum.* **2003**, *74* (8), 3597−3619.

(4) Sambur, J. B.; Chen, P. Approaches to Single-Nanoparticle Catalysis. *Annu. Rev. Phys. Chem.* **2014**, *65*, 395−422.

(5) Chen, P.; Zhou, X.; Andoy, N. M.; Han, K.-S.; Choudhary, E.; Zou, N.; Chen, G.; Shen, H. Spatiotemporal catalytic dynamics within single nanocatalysts revealed by single-molecule microscopy. *Chem. Soc. Rev.* **2014**, *43* (4), 1107−1117.

(6) Pujals, S.; Feiner-Gracia, N.; Delcanale, P.; Voets, I.; Albertazzi, L. Super-resolution microscopy as a powerful tool to study complex synthetic materials. *Nature Reviews Chemistry* **2019**, *3* (2), 68−84.

(7) Turkowyd, B.; Virant, D.; Endesfelder, U. From single molecules to life: microscopy at the nanoscale. *Anal. Bioanal. Chem.* **2016**, *408* (25), 6885−6911.

(8) Nicovich, P. R.; Owen, D. M.; Gaus, K. Turning single-molecule localization microscopy into a quantitative bioanalytical tool. *Nat. Protoc.* **2017**, *12* (3), 453−460.

(9) Xie, X. S.; Lu, H. P. Single-molecule Enzymology *. *J. Biol. Chem.* **1999**, *274* (23), 15967−15970.

(10) Chen, P.; Zhou, X.; Shen, H.; Andoy, N. M.; Choudhary, E.; Han, K.-S.; Liu, G.; Meng, W. Single-molecule fluorescence imaging of nanocatalytic processes. *Chem. Soc. Rev.* **2010**, *39* (12), 4560−4570.

(11) Liu, C.; Kubo, K.; Wang, E.; Han, K.-S.; Yang, F.; Chen, G.; Escobedo, F. A.; Coates, G. W.; Chen, P. Single polymer growth dynamics. *Science* **2017**, *358* (6361), 352−355.

(12) Galbraith, C. G.; Galbraith, J. A. Super-resolution microscopy at a glance. *Journal of Cell Science* **2011**, *124* (10), 1607−1611.

(13) Shen, H.; Tauzin, L. J.; Baiyasi, R.; Wang, W.; Moringo, N.; Shuang, B.; Landes, C. F. Single Particle Tracking: From Theory to Biophysical Applications. *Chem. Rev.* **2017**, *117* (11), 7331−7376.

(14) Miller, H.; Zhou, Z.; Shepherd, J.; Wollman, A. J. M.; Leake, M. C. Single-molecule techniques in biophysics: a review of the progress in methods and applications. *Rep. Prog. Phys.* **2018**, *81* (2), No. 024601.

(15) Tamarat, P.; Maali, A.; Lounis, B.; Orrit, M. Ten Years of Single-Molecule Spectroscopy. *J. Phys. Chem. A* **2000**, *104* (1), 1−16.

(16) Miles, B. N.; Ivanov, A. P.; Wilson, K. A.; Doğan, F.; Japrung, D.; Edel, J. B. Single molecule sensing with solid-state nanopores:

novel materials, methods, and applications. *Chem. Soc. Rev.* **2013**, *42* (1), 15−28.
(17) Walt, D. R. Optical Methods for Single Molecule Detection and Analysis. *Anal. Chem.* **2013**, *85* (3), 1258−1263.
(18) Kador, L.; Latychevskaia, T.; Renn, A.; Wild, U. P. Absorption spectroscopy on single molecules in solids. *J. Chem. Phys.* **1999**, *111* (19), 8755−8758.
(19) Celebrano, M.; Kukura, P.; Renn, A.; Sandoghdar, V. Single-molecule imaging by optical absorption. *Nat. Photonics* **2011**, *5* (2), 95−98.
(20) Jiang; Bosnick, K.; Maillard, M.; Brus, L. Single Molecule Raman Spectroscopy at the Junctions of Large Ag Nanocrystals. *J. Phys. Chem. B* **2003**, *107* (37), 9964−9972.
(21) Zrimsek, A. B.; Chiang, N.; Mattei, M.; Zaleski, S.; McAnally, M. O.; Chapman, C. T.; Henry, A.-I.; Schatz, G. C.; Van Duyne, R. P. Single-Molecule Chemistry with Surface- and Tip-Enhanced Raman Spectroscopy. *Chem. Rev.* **2017**, *117* (11), 7583−7613.
(22) Hu, C.; Tahir, R.; Mao, H. Single-Molecule Mechanochemical Sensing. *Acc. Chem. Res.* **2022**, *55* (9), 1214−1225.
(23) Koirala, D.; Yangyuoru, P. M.; Mao, H. Mechanical affinity as a new metrics to evaluate binding events. *Reviews in Analytical Chemistry* **2013**, *32* (3), 197−208.
(24) Lu, J.; Fan, Y.; Howard, M. D.; Vaughan, J. C.; Zhang, B. Single-Molecule Electrochemistry on a Porous Silica-Coated Electrode. *J. Am. Chem. Soc.* **2017**, *139* (8), 2964−2971.
(25) Shen, H.; Xu, W.; Chen, P. Single-molecule nanoscale electrocatalysis. *Phys. Chem. Chem. Phys.* **2010**, *12* (25), 6555−6563.
(26) Xu, W.; Shen, H.; Kim, Y. J.; Zhou, X.; Liu, G.; Park, J.; Chen, P. Single-Molecule Electrocatalysis by Single-Walled Carbon Nanotubes. *Nano Lett.* **2009**, *9* (12), 3968−3973.
(27) Armani, A. M.; Kulkarni, R. P.; Fraser, S. E.; Flagan, R. C.; Vahala, K. J. Label-Free, Single-Molecule Detection with Optical Microcavities. *Science* **2007**, *317* (5839), 783−787.
(28) Zijlstra, P.; Paulo, P. M. R.; Orrit, M. Optical detection of single non-absorbing molecules using the surface plasmon resonance of a gold nanorod. *Nat. Nanotechnol.* **2012**, *7* (6), 379−382.
(29) Baaske, M. D.; Vollmer, F. Optical observation of single atomic ions interacting with plasmonic nanorods in aqueous solution. *Nat. Photonics* **2016**, *10* (11), 733−739.
(30) Mao, X.; Liu, C.; Hesari, M.; Zou, N.; Chen, P. Super-resolution imaging of non-fluorescent reactions via competition. *Nat. Chem.* **2019**, *11* (8), 687−694.
(31) Needham, L.-M.; Saavedra, C.; Rasch, J. K.; Sole-Barber, D.; Schweitzer, B. S.; Fairhall, A. J.; Vollbrecht, C. H.; Wan, S.; Podorova, Y.; Bergsten, A. J.; et al. Label-free detection and profiling of individual solution-phase molecules. *Nature* **2024**, *629* (8014), 1062−1068.
(32) Bankar, S. B.; Bule, M. V.; Singhal, R. S.; Ananthanarayan, L. Glucose oxidase — An overview. *Biotechnology Advances* **2009**, *27* (4), 489−501.
(33) Wilson, R.; Turner, A. P. F. Glucose oxidase: an ideal enzyme. *Biosens. Bioelectron.* **1992**, *7* (3), 165−185.
(34) Lu, H.; Yu, S.; Qin, F.; Ning, W.; Ma, X.; Tian, K.; Li, Z.; Zhou, K. A secretion-based dual fluorescence assay for high-throughput screening of alcohol dehydrogenases. *Biotechnol. Bioeng.* **2021**, *118* (4), 1605−1616.
(35) Lai, X.; Wang, R.; Li, J.; Qiu, G.; Liu, J.-B. A cascade reaction-based switch-on fluorescent sensor for Ce(iv) ions in real samples. *RSC Adv.* **2019**, *9* (38), 22053−22056.
(36) Zhao, J.; Wang, S.; Lu, S.; Bao, X.; Sun, J.; Yang, X. An Enzyme Cascade-Triggered Fluorogenic and Chromogenic Reaction Applied in Enzyme Activity Assay and Immunoassay. *Anal. Chem.* **2018**, *90* (12), 7754−7760.
(37) Velema, W. A.; Kool, E. T. Fluorogenic Templated Reaction Cascades for RNA Detection. *J. Am. Chem. Soc.* **2017**, *139* (15), 5405−5411.
(38) Pokhrel, P.; Ren, K.; Shen, H.; Mao, H. Mechanical Stability of DNA Corona Phase on Gold Nanospheres. *Langmuir* **2022**, *38* (44), 13569−13576.
(39) Zuo, L.; Ren, K.; Guo, X.; Pokhrel, P.; Pokhrel, B.; Hossain, M. A.; Chen, Z.-X.; Mao, H.; Shen, H. Amalgamation of DNAzymes and Nanozymes in a Coronazyme. *J. Am. Chem. Soc.* **2023**, *145* (10), 5750−5758.
(40) Ovesný, M.; Křížek, P.; Borkovec, J.; Švindrych, Z.; Hagen, G. M. ThunderSTORM: a comprehensive ImageJ plug-in for PALM and STORM data analysis and super-resolution imaging. *Bioinformatics* **2014**, *30* (16), 2389−2390.
(41) Chen, J.; Ma, Q.; Li, M.; Chao, D.; Huang, L.; Wu, W.; Fang, Y.; Dong, S. Glucose-oxidase like catalytic mechanism of noble metal nanozymes. *Nat. Commun.* **2021**, *12* (1), 3375.
(42) Shen, H.; Zhou, X.; Zou, N.; Chen, P. Single-Molecule Kinetics Reveals a Hidden Surface Reaction Intermediate in Single-Nanoparticle Catalysis. *J. Phys. Chem. C* **2014**, *118* (46), 26902−26911.
(43) Schlegel, N.; Wiberg, G. K. H.; Arenz, M. On the electrooxidation of glucose on gold: Towards an electrochemical glucaric acid production as value-added chemical. *Electrochim. Acta* **2022**, *410*, No. 140023.
(44) Moggia, G.; Kenis, T.; Daems, N.; Breugelmans, T. Electrochemical Oxidation of d-Glucose in Alkaline Medium: Impact of Oxidation Potential and Chemical Side Reactions on the Selectivity to d-Gluconic and d-Glucaric Acid. *ChemElectroChem.* **2020**, *7* (1), 86−95.
(45) Zheng, Y. L.; Mei, D.; Chen, Y.-X.; Ye, S. The redox reaction of hydrogen peroxide at an Au(100) electrode: Implications for oxygen reduction kinetics. *Electrochem. Commun.* **2014**, *39*, 19−21.
(46) Zuo, L.; King, H.; Hossain, M. A.; Farhana, F.; Kist, M. M.; Stratton, R. L.; Chen, J.; Shen, H. Single-Molecule Spectroscopy Reveals the Plasmon-Assisted Nanozyme Catalysis on AuNR@TiO2. *Chemical & Biomedical Imaging* **2023**, *1* (8), 760−766.
(47) Zuo, L.; Hossain, M. A.; Dubadi, R.; Kist, M. M.; Farhana, F.; Chen, J.; Jaroniec, M.; Shen, H. Fluorogenic Reaction Probes Defect Sites on Titanium Dioxide Nanoparticles. *ChemNanoMat* **2024**, *10* (7), No. e202400031.
(48) Zhou, X.; Andoy, N. M.; Liu, G.; Choudhary, E.; Han, K.-S.; Shen, H.; Chen, P. Quantitative super-resolution imaging uncovers reactivity patterns on single nanocatalysts. *Nat. Nanotechnol.* **2012**, *7* (4), 237−241.
(49) Andoy, N. M.; Zhou, X.; Choudhary, E.; Shen, H.; Liu, G.; Chen, P. Single-Molecule Catalysis Mapping Quantifies Site-Specific Activity and Uncovers Radial Activity Gradient on Single 2D Nanocrystals. *J. Am. Chem. Soc.* **2013**, *135* (5), 1845−1852.
(50) Xu, W.; Kong, J. S.; Yeh, Y.-T. E.; Chen, P. Single-molecule nanocatalysis reveals heterogeneous reaction pathways and catalytic dynamics. *Nat. Mater.* **2008**, *7* (12), 992−996.
(51) Xu, W.; Kong, J. S.; Chen, P. Single-Molecule Kinetic Theory of Heterogeneous and Enzyme Catalysis. *J. Phys. Chem. C* **2009**, *113* (6), 2393−2404.
(52) Han, K. S.; Liu, G.; Zhou, X.; Medina, R. E.; Chen, P. How Does a Single Pt Nanocatalyst Behave in Two Different Reactions? *A Single-Molecule Study. Nano Letters* **2012**, *12* (3), 1253−1259.
(53) Lu, H. P.; Xun, L.; Xie, X. S. Single-Molecule Enzymatic Dynamics. *Science* **1998**, *282* (5395), 1877−1882.

https://doi.org/10.1021/cbmi.4c00114
Chem. Biomed. Imaging 2025, 3, 253−259